Nanocrystallinity and the Ordering of Nanoparticles in Two-Dimensional Superlattices: Controlled Formation of Either Core/Shell (Co/CoO) or Hollow CoO Nanocrystals

Zhijie Yang,[†] Isabelle Lisiecki,[†] Michael Walls,[‡] and Marie-Paule Pileni[†,*]

[†]Laboratoire des Matériaux Mésoscopiques et Nanométriques, UMR CNRS 7070, Université P. et M. Curie Bât F, 4 Place Jussieu, 75005 Paris, France and [‡]Laboratoire de Physique des Solides, UMR 8502, Université Paris-Sud, Bât. 510, 91405 Orsay Cedex, France

ABSTRACT Here it is demonstrated that the diffusion process of oxygen in Co nanoparticles is controlled by their 2D ordering and crystallinity. The crystallinity of isolated Co nanoparticles deposited on a substrate does not play any role in the oxide formation. When they are self-assembled in 2D superlattices, the oxidation process is slowed and produces either core/shell (Co/CoO) nanoparticles or hollow CoO nanocrystals. This is attributed to the decrease in the oxygen diffusion rate when the nanoparticles are interdigitated. Initially, polycrystalline nanoparticles form core/shell (Co/CoO) structures, while for single-domain hexagonal close-packed Co nanocrystals, the outward diffusion of Co ions is favored over the inward diffusion of oxygen, producing hollow CoO single-domain nanocrystals.

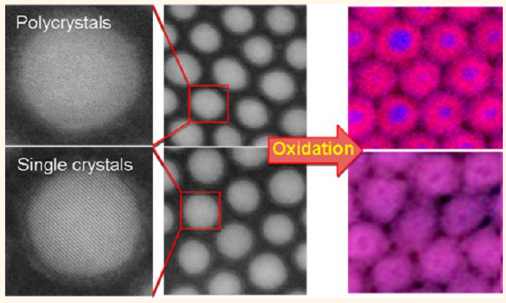

KEYWORDS: Co nanoparticles · nanocrystallinity · 2D ordering effect · core/shell structures · hollow structures · STEM · EELS

During the past few years, considerable effort has been put into the design and fabrication of nanomaterials exhibiting unique chemical and physical properties.[1−7] Tailoring the properties of nanoparticles through control of composition, size, shape, and crystal structure is the current trend in nanomaterial synthesis.[8−10] Co and its oxides are among the most promising materials for technological applications, including information storage, Li-ion batteries, magnetic fluids, spintronics, and catalysis.[11−14] Recently, Yin *et al.* employed Co nanocrystals as a starting material to demonstrate that hollow CoO nanocrystals can be successfully synthesized through the nanoscale Kirkendall effect, opening a new path for the design of such structures.[15]

The control of the nanoparticle crystallinity (called nanocrystallinity) has received much less attention and remains an open question.[16,17] In spite of the difficulties in synthesizing well-structured nanocrystals, various studies of their physical properties have been carried out over the past few years. One of the most highly developed research areas concerns the influence of the nanocrystallinity on the acoustic vibrational properties of the nanocrystals. Two models were developed from which it is expected that the breathing mode remains mostly unchanged, regardless of the nanocrystallinity.[18,19] This was recently confirmed experimentally for both Co and Au nanocrystals.[20,21] However, it is to be noted that these results are in contradiction with those reported by Tang *et al.*[16] for 10 nm Ag nanocrystals, whose breathing mode frequency was dependent on the nanocrystallinity. The quadrupolar vibrational mode (l = 2) of nanocrystals, easily detected through their low-frequency Raman scattering, is split into two-fold degenerate E_g modes and three-fold degenerate T_{2g} modes for single-domain nanocrystals.[22,23] In contrast, polycrystals exhibit only one band due to light scattering induced by their quadrupolar vibrational modes.[24] Some

* Address correspondence to marie-paule.pileni@upmc.fr.

Received for review October 23, 2012 and accepted December 31, 2012.

Published online January 11, 2013
10.1021/nn304922s

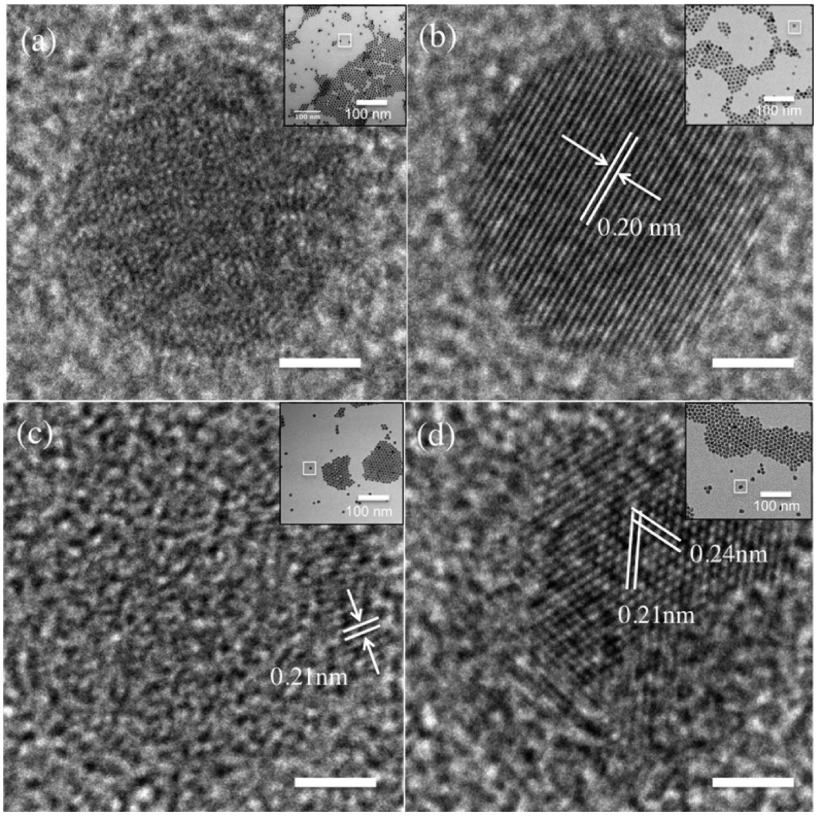

Figure 1. HRTEM images of a native Co nanocrystal (a) and after dry-phase annealing (b); native Co (c) and as-annealed (d) isolated Co nanocrystals after oxidation treatment. The insets are the corresponding low-magnification TEM images for reference, and the HRTEM image corresponds to the zone in the white rectangle. The scale bars all are 2 nm.

controversies have emerged regarding the mechanical properties of nanocrystals and the differences that might originate from their nanocrystallinity. Tang *et al.*[16] suggested an increase in the Young's modulus, deduced from the changes in the fundamental breathing mode for 10 nm Ag nanocrystals. The study of the compressibility of 10 nm Ag and 30 nm Au nanoparticles confirms a significantly higher stiffness than in the corresponding bulk phase, such behavior being attributed to the presence of twinned defects.[25] One model concerning the influence of the nanocrystallinity on the chemical properties of nanocrystals has been proposed; the formation of hollow Ag_2Se nanoparticles from single-domain 10 nm Ag nanocrystals has been observed, whereas completely solid Ag_2Se is obtained from MTP nanocrystals.[16] Furthermore, the different nanocrystallinities of Pt nanoparticles were shown to have a nontrivial influence on the electrochromism of TiO_2.[26] These divergences in the results can be easily explained by the very great difficulty in producing separately either single-domain nanocrystals or polycrystalline nanoparticles. There is thus clearly a need to develop new approaches for nanocrystallinity selection. There are surprisingly few reports concerning the intrinsic chemical properties resulting from 2D nanocrystal ordering. To our knowledge, the only studies are from our group.[27−30] In fact, we demonstrated an increase in the nanocrystals' stability with the level of ordering. By subjecting a self-assembled 2D array of Ag nanocrystals to oxygen plasma *via* a reactive ion etching process, it has been demonstrated that better ordered self-assemblies remain unchanged, while less ordered structures coalesce into larger nanocrystals with spheroidal shapes.[27,28] This technique could be a useful but destructive tool for detecting defects in 2D nanocrystal assemblies, which are usually limited to the local scale. The stability with respect to oxidation of Co nanocrystals markedly increases when they are self-ordered in compact hexagonal networks. This is attributed to the nanocrystal ordering that provides a substantial decrease in the permeability of the alkyl chain layer surrounding the particles.[29,30] Thus 2D arrays consisting of Co_{hcp}/CoO core/shell nanocrystals with a hexagonal close-packed (hcp) core were obtained by exposing the sample to air for 2.5 h after being annealed, whereas the polycrystalline nanoparticles are highly stable to an exposure to air even over several days.

To our knowledge, this is the first report of an intrinsic property related to the crystalline structure of nanoparticles which are self-ordered into a compact hexagonal network. Drastic changes in the oxidation processes occur as a function of the Co nanoparticles' crystallinities. It was found that either Co/CoO core/shell

or pure CoO structures were formed upon subjecting the polycrystalline Co nanoparticles to oxidation, whereas CoO hollow structures are generated starting from Co hcp single-domain nanocrystals. Furthermore, nanocrystals with 2D ordering display a different oxidation behavior from that of isolated nanocrystals (0D).

RESULTS AND DISCUSSION

Upon deposition of the native polycrystalline Co nanoparticles on a transmission electron microscopy (TEM) grid covered with a layer of amorphous carbon, the nanoparticles are either 2D self-organized or isolated. The average diameter and size distribution of the native Co nanoparticles, determined by measuring more than 500 particles imaged by TEM, are 7.2 nm and 10%, respectively (Supporting Information, Figure S1a). Figure 1a is a high-resolution TEM (HRTEM) image showing that a few small crystalline domains with a typical size smaller than 1 nm constitute the nanoparticle. After annealing at 250 °C in an inert argon atmosphere, nearly all of the Co nanoparticles are transformed from a polycrystalline face-centered cubic (fcc) to a single-domain hcp structure (Figure 1b). The average diameter and size distribution of the nanocrystals after annealing remains unchanged compared to that of the native state (Supporting Information, Figure S1b). Under such experimental conditions, the surfactant molecules used as coating agents are partially destroyed with the probable formation of carbon layers. However, similar end products are obtained from nanocrystals annealed in solution, indicating that this carbonization process does not affect the results (see below). The choice of the dry system developed below is because of the better nanocrystal ordering with as-annealed nanoparticles than that found in nanocrystals produced in solution. The improved crystallinity is well illustrated by the HRTEM image inset in Figure 1b, which clearly shows a set of interplanar spacings at 0.20 nm that is indexed as the (002) reflection of the hcp Co lattice. Electron diffraction patterns confirm the formation of hcp Co nanocrystals. Note that it is not possible to use X-ray diffraction because of the very small amounts of material available. These data confirm those published previously.[31]

The two samples of polycrystalline nanoparticles and single-domain nanocrystals are simultaneously placed in a modified Schlenk line setup (Scheme 1a). They are subjected to an oxygen flow and heated to 200 °C. After aging for 10 min, the heating system is removed and an argon flow is introduced in order to stop the intense oxidation process. As mentioned, the TEM grids contain well-defined monolayers with some isolated nanoparticles, allowing us to study separately the behavior of isolated and self-ordered nanoparticles with differing crystalline structures (polycrystals and single domains). Several questions concerning the oxidation of these Co nanoparticles can be raised: (i)

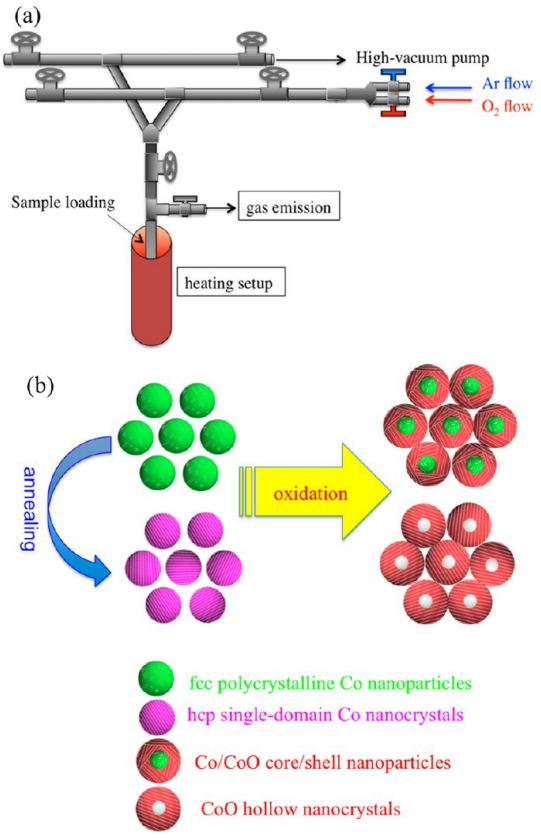

Scheme 1. (a) Modified Schlenk line setup used for the air-free annealing or oxidizing of the samples; (b) schematic illustration of oxidation behavior of 2D hexagonally ordered Co nanoparticles differing by their nanocrystallinity.

What is the role of the crystalline structure of these nanoparticles on the oxidation rate? (ii) Does the nanoparticle ordering play a role in the oxidation process? (iii) Does the crystalline structure of the nanoparticles in a self-ordered compact hexagonal network determine the material produced? To answer these questions, we will first consider the isolated nanoparticles with differing crystallinities and then do the same for 2D-ordered arrays.

Isolated Nanoparticles Differing by Their Crystallinities. HRTEM images of isolated nanoparticles of different initial crystallinities and having undergone oxidation are shown in Figure 1c,d, respectively. In both cases, a few lattice planes of 0.21 nm are observed and could be indexed as CoO. The average diameter of the particles produced from polycrystalline or single-domain nanocrystals is increased from 7.2 to 9.9 nm. The size distributions of the oxidized nanoparticles derived from polycrystalline and single-domain nanoparticles are 10 and 12%, respectively (Supporting Information, Figure S2). These data clearly indicate that the oxidation of isolated nanoparticles is essentially independent of their initial crystalline structure. To confirm this claim, the structure of the samples after oxidation is investigated by scanning transmission electron microscopy (STEM), where multiple signals can be collected,

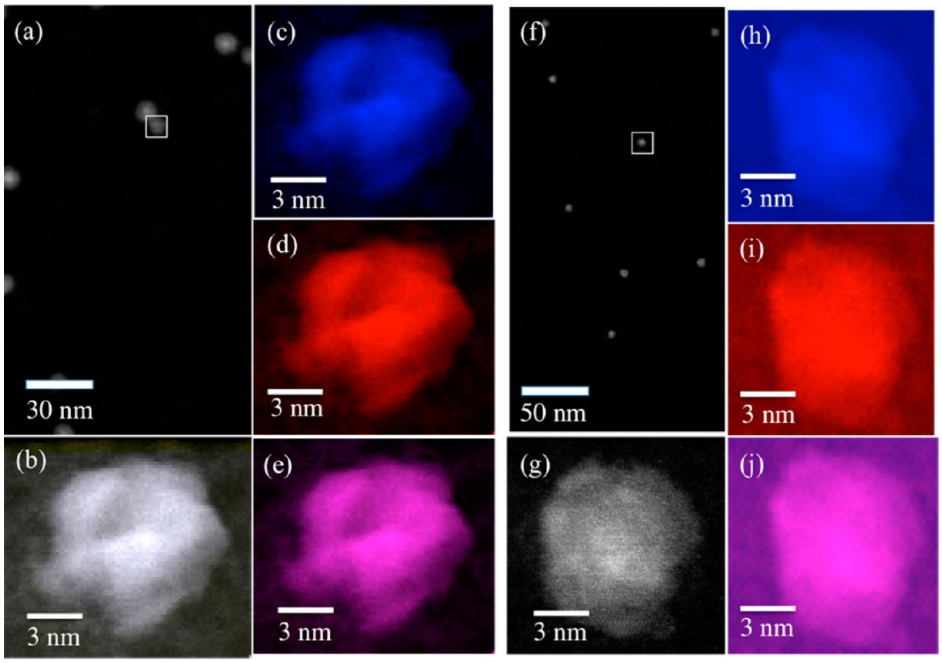

Figure 2. STEM images of isolated nanocrystals after oxidation: (a) HAADF-STEM image of polycrystalline Co after oxidation; (b) summed spectrum image taken from the rectangle from (a); (c) elemental map for cobalt, using the Co L-edge; (d) elemental map for oxygen, using the O K-edge; (e) superposition of cobalt and oxygen maps. (f) HAADF-STEM image of single-domain hcp Co after oxidation; (g) summed spectrum image taken from the rectangle from (f); (h) elemental map for cobalt, using the Co L-edge; (i) elemental map for oxygen, using the O K-edge; (j) superposition of cobalt and oxygen maps.

including the bright-field (BF) and high-angle annular dark-field (HAADF) or *Z*-contrast images, along with spectroscopic signals—in our case, the electron energy loss spectrum (EELS). Figure 2 shows typical STEM images of isolated nanoparticles from both the polycrystalline and single-domain phases after oxidation. Figure 2a is a HAADF image of several isolated polycrystalline Co nanoparticles, which is used as a reference to record a spectrum image. Figure 2b is the summed spectrum image from the selected area in Figure 2a, from which chemical maps for cobalt and oxygen, using, respectively, the Co L-edge (Figure 2c) and O K-edge (Figure 2d), are collected. The chemical maps of the isolated nanoparticle clearly show similar and homogeneous contrasts throughout the nanoparticle. The superimposition of the two signals exhibits a uniform purple pattern of pure Co_xO_y (Figure 2e). Note that the shape of the isolated nanoparticle has become irregular, and a surface hole is also observed, indicating that a surface reconstruction induced by the oxidation process occurs in spite of the surface coating of organics. STEM images of isolated nanocrystals from the hcp phase after oxidation are presented in Figure 2f–j, and the chemical maps of one nanocrystal are generated from the summed spectrum image of Figure 2g. As with polycrystalline Co nanoparticles, homogeneous contrasts are obtained at the Co L-edge (Figure 2h) and O K-edge (Figure 2i). The superimposed Co and O signals (Figure 2j) indicate a pure Co_xO_y structure. For both samples, the corresponding EELS profiles are shown in Figure S3 (Supporting Information), from which one can observe peaks assigned to the O K-edge and the Co L-edge, respectively. No significant prepeak at 535 eV can be observed. This is a nontrivial difference between CoO and Co_3O_4 and is attributed to the hybridization of the O 2p state with the Co 3d; the increase in the O K-edge prepeak intensity in Co_3O_4 compared to CoO is due to the larger number of unoccupied Co 3d states in Co_3O_4. EELS spectral analysis thus further confirms that the as-formed oxides are CoO, which is in agreement with the HRTEM result. On the basis of the above STEM analysis, we can conclude that the oxidation behavior of isolated nanoparticles does not depend on the nanocrystallinity and results in the fully oxidized solid CoO structures. Note that in both cases deformation of the surface of CoO nanoparticles takes place. The experiments were repeated on a large number of isolated nanoparticles, and the data are highly reproducible.

At this point, we can consider the questions (ii) and (iii) proposed above. In brief, they concern the influence of the nanoparticle crystallinity on the oxidation process when the particles are self-ordered into 2D superlattices.

Self-Ordered 2D Hexagonal Networks of Polycrystalline Nanoparticles. Figure 3a shows a TEM image of self-ordered polycrystalline Co nanoparticles freshly deposited on a grid. Figure 3c shows that after oxidation the 2D array remains ordered. However, the nanoparticles' contrasts are no longer homogeneous and exhibit a core/shell structure. No coalescence between particles is observed. However, from time to time, we observe CoO

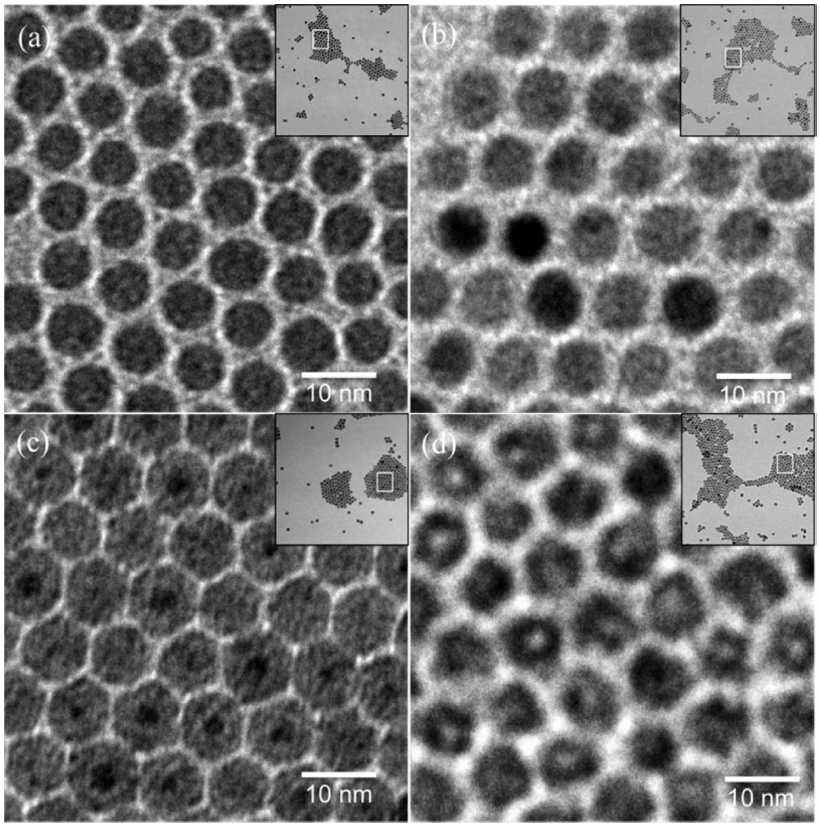

Figure 3. TEM images of 2D hexagonally organized nanoparticles: (a) polycrystalline Co and (b) single-crystalline hcp Co; (c,d) corresponding TEM images of polycrystalline and single-crystalline hcp Co after oxidation. The inset is the corresponding low-magnification TEM image as reference, and the enlarged image is selected from the white rectangle.

nanoparticles touching each other, probably because of the expansion of the Co nanoparticles subjected to oxidation as observed above for isolated nanoparticles.

Figure 4 shows the simultaneously acquired BF and HAADF images of the nanoparticles after oxidation. The HAADF intensity is a function of atomic number as well as thickness. The atomic numbers of the constituent elements O ($Z = 8$) and Co ($Z = 27$) are substantially different, so the elemental Z-contrast intensity can be considered useful for the observation of these hetero-nanostructures. Figure 4a shows a HAADF-STEM image of an ordered area of oxidized polycrystalline Co nanoparticles. The inner part of the nanoparticles is brighter in the beam direction, whereas the outer part is darker, indicating the non-uniform elemental distribution. The uneven "core" part of the nanoparticles demonstrates that the oxidation process varies between different Co nanoparticles. A magnified HAADF image (Figure 4b) indicates the well-crystallized "shell" part of the nanoparticle, and the lattice fringe spacings are determined to be 0.21 nm, which is in good agreement with the (200) plane of the CoO cubic phase. Various other CoO lattice fringe spacings are also observed (Figure 4c,d).

A panoramic HAADF-STEM image of hexagonally ordered oxidized Co nanoparticles is shown in Figure 5a. The local chemical maps are shown in Figure 5b–d. The Co signal (in blue) is present throughout the nanoparticles and is markedly enhanced in their central region (Figure 5b). Conversely, the oxygen signal (in red) is mainly located at the shell region of the nanoparticles (Figure 5c). The superposition of the two maps reveals a blue center and a purple edge, in agreement with a Co/CoO core/shell structure model, with shell thicknesses in the range of 2–4 nm (Figure 5d). The line profile across the center of the 2D superlattices records their elemental distribution. It clearly shows that the Co signal is not in phase with that of oxygen (Figure 5e). The Co profile has minima at the two peaks in the oxygen profile, indicating well-defined Co/CoO core/shell structures. From these data, it is clearly demonstrated that, in contrast to what is observed for isolated polycrystalline nanoparticles, self-assembled compact hexagonal layers form core/shell Co/CoO structures (see also Scheme 1b). These data slightly differ from those we previously obtained when using air as the oxidizing agent without a heating setup. In that case, the polycrystalline Co nanoparticles were perfectly stable against oxidation. Here, the modified Schlenk line, as described above, gives a better control of the oxygen flow, heating process, *etc*.

Single-Domain Nanocrystals Self-Ordered into a Compact Hexagonal Network. The same analysis has been performed on single-domain hcp Co nanocrystals. Surprisingly marked

changes appear. After oxidation, the TEM image (Figure 3d) reveals a hollow cavity inside the nanocrystal (also see Scheme 1b). The average size of the hollow nanocrystals increases from 7.2 nm (before oxidation) to 8.3 nm (Supporting Information, Figure S4). This increase is slightly smaller than that occurring in the polycrystalline Co/CoO nanoparticles after oxidation. Although no coalescence is observed, the contours of the hollow nanocrystals turn out to be irregular, indicating that the oxidation process is non-uniform. The formation of a single void inside the nanocrystals is generally attributed to the nanoscale Kirkendall effect, which has proven to be a versatile method for the generation of vacancies inside inorganic nanocrystals. When Co nanocrystals are exposed to oxygen at high temperature (200 °C), an oxide layer is instantly formed on their surface. Because the outward diffusion of Co ions in this oxide layer is much faster than the inward diffusion of oxygen, an inward flux of vacancies will result in the formation of interior nanocavities at the Co/oxide interface. With the depletion of the Co atoms accompanied by the condensation of several nanocavities into a single large cavity, completely hollow cobalt oxide nanocrystals with a single large cavity are formed. This evolution mechanism is similar to that described in a previous report starting with ε phase Co nanocrystals.[15] The STEM images of single-domain self-ordered compact hexagonal arrays of hcp

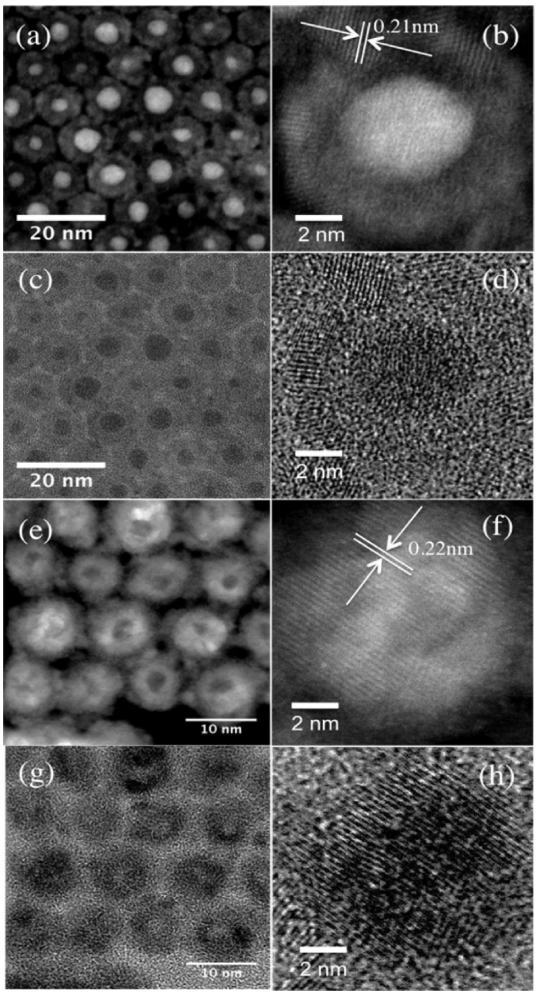

Figure 4. (a,b) HAADF-STEM and (c,d) BF-STEM images of 2D-organized Co polycrystals after oxidation; (e,f) HAADF-STEM and (g,h) BF-STEM images of 2D-organized hcp Co single-domain crystals after oxidation.

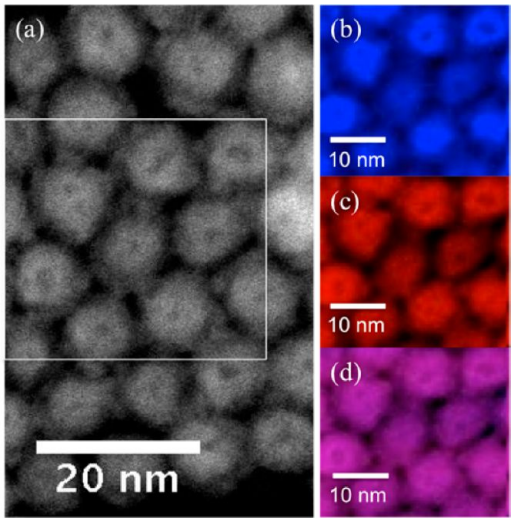

Figure 6. HAADF-STEM image of 2D-organized hcp Co single-domain crystals after oxidation; (b,c) cobalt and oxygen maps collected from the rectangular zone in panel (a); (d) superposition of the cobalt and oxygen maps.

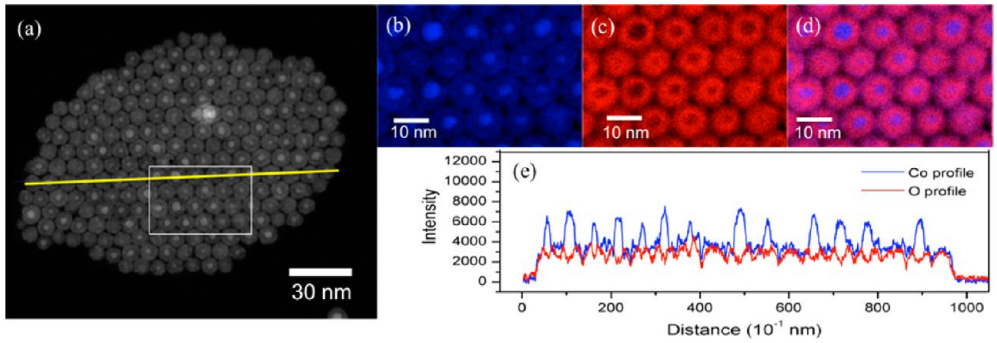

Figure 5. (a) HAADF-STEM image of 2D-organized Co polycrystals after oxidation; (b,c) cobalt and oxygen maps collected from the white rectangle in panel (a); (d) superposition of cobalt and oxygen maps; (e) line profile corresponding to the yellow line in panel (a).

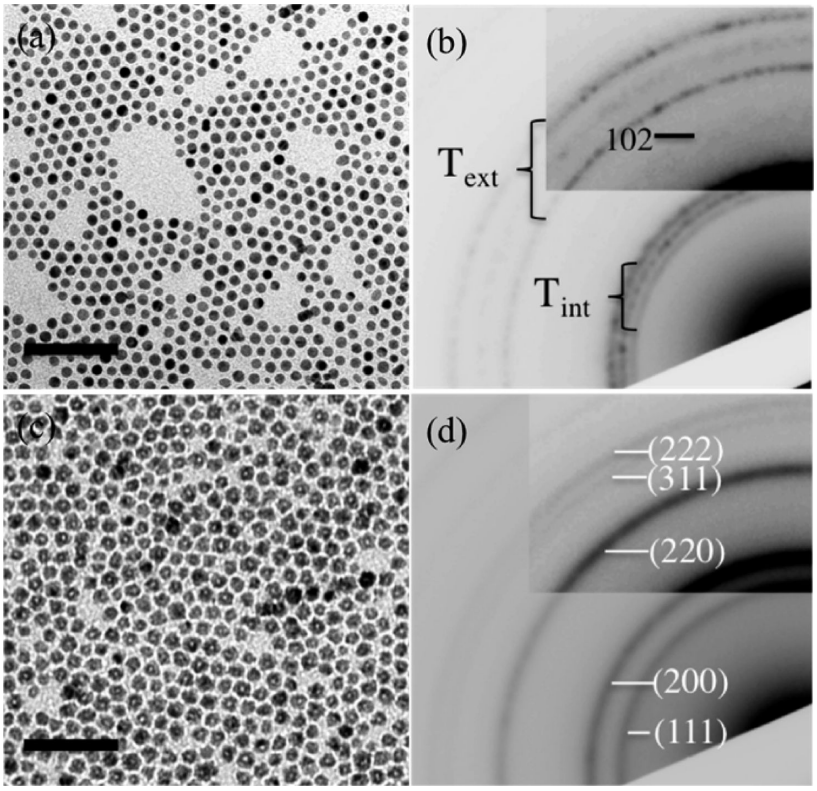

Figure 7. (a) TEM image of hcp Co nanocrystals obtained by solution-phase annealing, (c) after oxidation at 200 °C for 10 min. (b,d) Corresponding ED patterns before and after oxidation. The scale bars in (a) and (c) are 50 nm. T_{int} and T_{ext} marked on the ED pattern refer to the internal triplet rings [(100), (101), (002)] and external triplet rings [(110), (103), (112)], respectively.

confirm the drastic change in the final product. The *Z*-contrast HAADF image (Figure 4e) confirms the presence of a cavity in the nanocrystal. In addition, both high-resolution BF-STEM (Figure 4h) and HAADF-STEM (Figure 4f) images reveal that the hollow nanocrystals are well crystallized with lattice planes spaced at 0.22 nm, corresponding to (200) in cubic CoO. Note that, throughout the nanocrystal, a single domain of CoO remains present, contrary to what was observed with native nanoparticles, where polydomains are observed. Figure 6a shows the HAADF-STEM image of 2D-ordered nanocrystals produced from single-domain hcp nanocrystals. Panels b and c of Figure 6 show the Co and O projected distributions extracted from an EELS spectrum image, respectively. The Co (blue) and O (red) composite image demonstrates that the hollow nanocrystals are homogeneous in their chemical distribution. From these data, it is claimed that when single-domain Co nanocrystals are self-assembled in a compact hexagonal network, hollow CoO single-domain nanocrystals are produced. This suggests that both the interdigitation process and nanocrystallinity are key parameters in the formation of hollow nanocrystals. Here we underline the fact that the single-domain particles are produced by dry annealing (see the Methods section) and a degradation of the coating layer during the thermal treatment could take place, which might be thought to explain the big difference between polycrystalline nanoparticles and single-domain nanocrystals when self-assembled into compact hexagonal networks. To investigate this possibility, we also used a method described elsewhere,[32] in which the annealing process of polycrystal nanoparticles takes place in solution. At the end of the synthesis, the Co nanoparticles are dispersed in dioctylether and 5 mL of the colloidal solution is annealed at 250 °C for 60 min. Then, 0.8 mL of dodecanoic acid is added to the solution to prevent any nanocrystal coalescence. The TEM image of the annealed colloidal solution (Figure 7a) and its corresponding electron diffraction (ED) pattern (Figure 7c) confirm the results already obtained according to which single-domain hcp Co nanocrystals are produced. Such assemblies of nanocrystals are then subjected to the same treatment as those above. Figure 7b and the corresponding ED pattern (Figure 7d) show the formation of CoO hollow nanocrystals. This result allows us to conclude that a clear nanocrystallinity effect occurs during the oxidation of the self-organized 2D Co nanocrystal arrays.

CONCLUSIONS

It is well-known that the crystallinity of Co nanoparticles can be controlled over a range going from polycrystalline fcc Co to single-domain hcp Co nanocrystals. Here we have demonstrated that the nanocrystallinity of isolated nanoparticles does not play any role in the production of deformed polycrystalline CoO nanoparticles. This is probably due to oxygen diffusion

through the alkyl chains used to protect the nanocrystals against coalescence. Surprisingly, when these nanocrystals are self-ordered into a compact hexagonal network, the oxidation process markedly differs. This is attributed to the fact that the coating alkyl chains of the Co nanoparticles reduce the oxygen diffusion speed. Furthermore, the crystallinity of the nanoparticles remains the major determinant of the final product. Thus core/shell (Co/CoO) nanoparticles are formed by the oxidation of polycrystalline nanoparticles, whereas hollow CoO nanocrystals are obtained from single-domain hcp nanocrystals following the general mechanism of the nanoscale Kirkendall effect. This change in the final product is attributed to the fact that, when single-domain nanocrystals are formed, the outward diffusion process of Co atoms through an oxide layer is faster than the inward diffusion of oxygen.

METHODS

Chemicals. All materials were used without further purification: cobalt acetate, dodecanoic acid, sodium borohydride, and octylether are from Aldrich, isooctane and hexane from Fluka, sodium di(ethylhexyl)sulfosuccinate (NaAOT) from Sigma. The synthesis of cobalt(II) bis(2-ethylhexyl)sulfosuccinate ($Co(AOT)_2$) was described previously.[33]

Apparatus. Conventional transmission electron microscopy (TEM) was performed using a JEOL 1011 microscope at 100 kV. High-resolution transmission electron microscopy was performed using a JEOL 2010 microscope at 200 kV and using a Nion Ultrastem 100 scanning transmission electron microscope operating at 100 kV. Scanning TEM (STEM) images were taken using a high-angle annular dark-field (HAADF) detector. The probe convergence, EELS collection, and inner and outer HAADF detector angles were 34, 50, 75, and 210 mrad, respectively. Spectrum images were denoised *via* principal components analysis using the Hyperspy software suite.[34,35]

Synthesis. The synthesis and characterization of Co polycrystals coated with dodecanoic acid have been described in a previous paper:[33] reverse micelles of 5×10^{-2} M $Co(AOT)_2$ form an isotropic phase. The amount of water added in solution is fixed to reach a water concentration defined as $w = [H_2O]/[AOT] = 32$. Sodium borohydride, $NaBH_4$, added to the micellar solution reduces the cobalt ions. The sodium borohydride content is defined as $R = [NaBH_4]/[Co(AOT)_2] = 6$. Immediately after $NaBH_4$ addition, the micellar solution color changes from pink to black, indicating the formation of colloidal Co nanocrystals. The nanocrystals are coated and then extracted from the surfactant. The coating process is as follows: 0.2 M lauric acid, $C_{11}H_{23}COOH$, is added to the solution containing nanocrystals, surfactants, water, and isooctane, inducing a chemical bond between the oxygen of dodecanoic acid and the Co atoms located at the interface. The coated Co nanocrystals are then washed and centrifuged several times with ethanol to remove all of the AOT surfactant, and the black powder obtained is dispersed in hexane. In order to eliminate the largest nanocrystals formed, the solution is again centrifuged and only the upper part containing the smallest sized nanocrystals is collected. At the end of the synthesis, ~7 nm cobalt nanocrystals coated with dodecanoic acid with a ~10% size distribution are produced. The entire synthesis is carried out in a N_2 glovebox using deoxygenated solvents to prevent particle oxidation.

Dry-Phase Annealing and Oxidation of the Samples. After deposition of the native Co nanocrystals solution on the TEM grids, the samples were loaded into the oxidation apparatus, which is illustrated in Scheme 1. The oxidation apparatus was based on a modified Schlenk line, including high-vacuum pump, source of inert gas (Ar), and source of oxygen gas (O_2). After loading into the apparatus, the samples were subjected to the vacuum pump Ar flow three times in order to remove the air. The heating setup was preadjusted to 250 °C to anneal the samples. The annealing process takes place under an argon flux, whose rate is determined by gas bubbles (2 bubbles/s). After 60 min aging at 250 °C, the heating setup was removed in order to stop the annealing process. When the samples were subjected to pure oxygen, the heating setup was preadjusted to 200 °C. After 10 min, the heating setup was removed and the oxygen flow was replaced by an argon flow in order to stop the oxidation immediately. After cooling by an argon flow to room temperature, the samples were characterized by TEM and STEM.

Solution-Phase Annealing and Oxidation of the Samples. The native Co nanocrystals were annealed at 250 °C. The solvent used was octylether, whose boiling point is 286 °C. Two milliliters of 10^{-2} M of the colloidal solution resulting from the synthesis was first evaporated to remove the original solvent (hexane). Then, the powder was redispersed in 5 mL of octylether. The annealing treatment took place in a refluxing bath. This is a four-necked flask allowing a nitrogen flux, the control of the solution temperature, the injection and the withdrawing of the solution with a syringe in order to avoid any oxidation of cobalt, and the refluxing of the solvent during the heating step. The solution was heated to the required temperature with a heating rate of 10 °C per minute up to 140 °C then more slowly with a heating rate of 2 °C per minute. Once the temperature was reached, it was maintained for 60 min and then cooled under stirring. Then, using the syringe, the sample was removed from the flask and placed inside a glovebox under a N_2 flux. Then, 0.8 mL of 5×10^{-3} M dodecanoic acid was added in order to avoid aggregation of the nanocrystals. The solution was left overnight and then subjected to cleaning cycles *via* suspension in ethanol and centrifugation twice to ensure a complete removal of octylether and dodecanoic acid in excess. Finally, the nanocrystals were dispersed in 0.5 mL of hexane. The annealing treatment and all other steps occurred under a N_2 flux.

Conflict of Interest: The authors declare no competing financial interest.

Acknowledgment. The research leading to these results has been supported by an Advanced Grant of the European Research Council under Grant 267129. The authors wish to thank the French MET and atom-probe network METSA. Z.J.Y. thanks the China Scholarship Council for financial support.

Supporting Information Available: Size histograms of the nanocrystals before and after oxidation; EELS spectra of the nanocrystals after oxidation. This material is available free of charge *via* the Internet at http://pubs.acs.org.

REFERENCES AND NOTES

1. Pileni, M. P. Reverse Micelles as Microreactors. *J. Phys. Chem.* **1993**, *97*, 6961–6973.
2. Pileni, M. P. Nanosized Particles Made in Colloidal Assemblies. *Langmuir* **1997**, *13*, 3266–3276.
3. Murray, C. B.; Sun, S. H.; Gaschler, W.; Doyle, H.; Betley, T. A.; Kagan, C. R. Colloidal Synthesis of Nanocrystals and Nanocrystal Superlattices. *IBM J. Res. Dev.* **2001**, *45*, 47–56.
4. Pileni, M. P. Nanocrystal Self-Assemblies: Fabrication and Collective Properties. *J. Phys. Chem. B* **2001**, *105*, 3358–3371.
5. Pileni, M. P. The Role of Soft Colloidal Templates in Controlling the Size and Shape of Inorganic Nanocrystals. *Nat. Mater.* **2003**, *2*, 145–150.
6. Arico, A. S.; Bruce, P.; Scrosati, B.; Tarascon, J.-M.; van Schalkwijk, W. Nanostructured Materials for Advanced Energy Conversion and Storage Devices. *Nat. Mater.* **2005**, *4*, 366–377.
7. Jain, P. K.; Huang, X. H.; El-Sayed, I. H.; El-Sayed, M. A. Noble Metals on the Nanoscale: Optical and Photothermal

Properties and Some Applications in Imaging, Sensing, Biology, and Medicine. *Acc. Chem. Res.* **2008**, *41*, 1578–1586.
8. Sun, Y. G.; Xia, Y. N. Shape-Controlled Synthesis of Gold and Silver Nanoparticles. *Science* **2002**, *298*, 2176–2179.
9. Peng, X. G.; Manna, L.; Yang, W. D.; Wickham, J.; Scher, E.; Kadavanich, A.; Alivisatos, A. P. Shape Control of CdSe Nanocrystals. *Nature* **2000**, *404*, 59–61.
10. Park, J.; Joo, J.; Kwon, S. G.; Jang, Y.; Hyeon, T. Synthesis of Monodisperse Spherical Nanocrystals. *Angew. Chem., Int. Ed.* **2007**, *46*, 4630–4660.
11. Liang, Y.; Li, Y.; Wang, H.; Zhou, J.; Wang, J.; Regier, T.; Dai, H. Co_3O_4 Nanocrystals on Graphene as a Synergistic Catalyst for Oxygen Reduction Reaction. *Nat. Mater.* **2011**, *10*, 780–786.
12. Black, C. T.; Murray, C. B.; Sandstrom, R. L.; Sun, S. Spin-Dependent Tunneling in Self-Assembled Cobalt-Nanocrystal Superlattices. *Science* **2000**, *290*, 1131–1134.
13. Shaju, K. M.; Jiao, F.; Debart, A.; Bruce, P. G. Mesoporous and Nanowire Co_3O_4 as Negative Electrodes for Rechargeable Lithium Batteries. *Phys. Chem. Chem. Phys.* **2007**, *9*, 1837–1842.
14. Puntes, V. F.; Krishnan, K. M.; Alivisatos, A. P. Synthesis, Self-Assembly, and Magnetic Behavior of a Two-Dimensional Superlattice of Single-Crystal ε-Co Nanoparticles. *Appl. Phys. Lett.* **2001**, *78*, 2187–2189.
15. Yin, Y. D.; Rioux, R. M.; Erdonmez, C. K.; Hughes, S.; Somorjai, G. A.; Alivisatos, A. P. Formation of Hollow Nanocrystals through the Nanoscale Kirkendall Effect. *Science* **2004**, *304*, 711–714.
16. Tang, Y.; Ouyang, M. Tailoring Properties and Functionalities of Metal Nanoparticles through Crystallinity Engineering. *Nat. Mater.* **2007**, *6*, 754–759.
17. Zhang, Q. B.; Xie, J. P.; Yu, Y.; Yang, J. H.; Lee, J. Y. Tuning the Crystallinity of Au Nanoparticles. *Small* **2010**, *4*, 523–527.
18. Saviot, L.; Murray, D. B. Acoustic Vibrations of Anisotropic Nanoparticles. *Phys. Rev. B* **2009**, *79*, 214101.
19. Crut, A.; Maioli, P.; Del Fatti, N.; Vallee, F. Anisotropy Effects on the Time-Resolved Spectroscopy of the Acoustic Vibrations of Nanoobjects. *Phys. Chem. Chem. Phys.* **2009**, *11*, 5882–5888.
20. Polli, D.; Lisiecki, I.; Portales, H.; Cerullo, G.; Pileni, M. P. Low Sensitivity of Acoustic Breathing Mode Frequency in Co Nanocrystals upon Change in Nanocrystallinity. *ACS Nano* **2011**, *5*, 5785–5791.
21. Goubet, N.; Yan, C.; Polli, D.; Portales, H.; Arfaoui, I.; Cerullo, G.; Pileni, M. P. Modulating Physical Properties of Isolated and Self-Assembled Nanocrystals through Change in Nanocrystallinity. *Nano Lett.* **2012**, DOI: 10.1021/nl303898y.
22. Portales, H.; Goubet, N.; Saviot, L.; Adichtchev, S.; Murray, D. B.; Mermet, A.; Duval, E.; Pileni, M. P. Probing Atomic Ordering and Multiple Twinning in Metal Nanocrystals through Their Vibrations. *Proc. Natl. Acad. Sci. U.S.A.* **2008**, *105*, 14784–14789.
23. Portales, H.; Goubet, N.; Saviot, L.; Yang, P.; Sirotkin, S.; Duval, E.; Mermet, A.; Pileni, M. P. Crystallinity Dependence of the Plasmon Resonant Raman Scattering by Anisotropic Gold Nanocrystals. *ACS Nano* **2010**, *4*, 3489–3497.
24. Portales, H.; Saviot, L.; Duval, E.; Fujii, M.; Hayashi, S.; Del Fatti, N.; Vallee, F. Resonant Raman Scattering by Breathing Modes of Metal Nanoparticles. *J. Chem. Phys.* **2001**, *115*, 3444.
25. Gu, Q. F.; Krauss, G.; Steurer, W.; Gramm, F.; Cervellino, A. Unexpected High Stiffness of Ag and Au Nanoparticles. *Phys. Rev. Lett.* **2008**, *100*, 045502-1/4.
26. Park, K.-W. Influence of Pt Nanocrystallinity on Electrochromism of TiO_2. *Inorg. Chem.* **2005**, *44*, 3190–3193.
27. Klecha, E.; Ingert, D.; Walls, M.; Pileni, M. P. Immunity of Coated Self-Ordered Silver Nanocrystals: A New Intrinsic Property Due to the Nanocrystal Ordering. *Langmuir* **2009**, *25*, 2824–2830.
28. Klecha, E.; Arfaoui, I.; Richardi, J.; Ingert, D.; Pileni, M. P. 2D Silver Nanocrystal Ordering Modulated by Various Substrates and Revealed Using Oxygen Plasma Treatment. *Phys. Chem. Chem. Phys.* **2011**, *13*, 2953–2962.
29. Lisiecki, I.; Walls, M.; Parker, D.; Pileni, M. P. 2D Self-Organization of Core/Shell Co_{hcp}/Co Nanocrystals. *Langmuir* **2008**, *24*, 4295–4299.
30. Lisiecki, I.; Turner, S.; Bals, S.; Pileni, M. P.; Van Tendeloo, G. The Remarkable and Intriguing Resistance to Oxidation of 2D Ordered hcp Co Nanocrystals. A New Intrinsic Property. *Chem. Mater.* **2009**, *21*, 2335–2338.
31. Lisiecki, I.; Salzemann, C.; Parker, D.; Albouy, P. A.; Pileni, M. P. Emergence of New Collective Properties of Cobalt Nanocrystals Ordered in fcc Supracrystals: I, Structural Investigation. *J. Phys. Chem. C* **2007**, *111*, 12625–12631.
32. Yang, Z.; Cavalier, M.; Walls, M.; Bonville, P.; Lisiecki, I.; Pileni, M.-P. A Phase-Solution Annealing Strategy To Control the Cobalt Nanocrystal Anisotropy: Structural and Magnetic Investigations. *J. Phys. Chem. C* **2012**, *116*, 15723–15730.
33. Lisiecki, I.; Pileni, M. P. Synthesis of Well-Defined and Low Size Distribution Cobalt Nanocrystals: The Limited Influence of Reverse Micelles. *Langmuir* **2003**, *19*, 9486–9489.
34. Arenal, R.; de la Peña, F.; Stéphan, O.; Walls, M.; Tencé, M.; Loiseau, A.; Colliex, C. Extending the Analysis of EELS Spectrum-Imaging Data, from Elemental to Bond Mapping in Complex Nanostructures. *Ultramicroscopy* **2008**, *109*, 32–38.
35. de la Peña, F.; Berger, M.-H.; Hochepied, J.-F.; Dynys, F.; Stephan, O.; Walls, M. Mapping Titanium and Tin Oxide Phases Using EELS: An Application of Independent Component Analysis. *Ultramicroscopy* **2011**, *111*, 169–176.